Non-polynomial spline alternatives in Isogeometric Symmetric Galerkin BEM

Non-polynomial spline alternatives in Isogeometric Symmetric Galerkin BEM

A. Aimi[a], M. Diligenti[a], M. L. Sampoli[b], A. Sestini[c,*]

[a]*Department of Mathematics and Computer Science, University of Parma, Parco Area delle Scienze, 53/A, Parma, Italy*
[b]*Department of Information Engineering and Mathematics, University of Siena, Via Roma 56, Siena, Italy*
[c]*Department of Mathematics and Computer Science, University of Florence, Viale Morgagni 67, Firenze, Italy*

Abstract

The application of the Isogeometric Analysis (IgA) paradigm to Symmetric Galerkin Boundary Element Method (SGBEM) is investigated. In order to obtain a very flexible approach, the study is here developed by using non polynomial spline functions to represent both the domain boundary and the approximate solution. The numerical comparison between IGA-SGBEM and both curvilinear and standard SGBEM approaches shows the general capability of the presented method to produce accurate approximate solutions with less degrees of freedom.

Keywords: Generalized B-splines, NURBS, Isogeometric Analysis, Symmetric Galerkin Boundary Element Method

1. Introduction

Boundary element methods (BEMs) [5] are nowadays considered a valid alternative to classical domain methods, such as finite differences (FDMs) [24] and finite elements (FEMs) [13], above all in physical and engineering applications involving, for instance, problems defined on unbounded domains with bounded boundary. If the fundamental solution of the differential operator at hand is known, a wide class of elliptic, parabolic, hyperbolic, interior and exterior problems can be reformulated by integral equations defined on the boundary of the given spatial domain, whose approximate solution is successively obtained by collocation or Galerkin BEMs. In the last decades, collocation BEM has been the subject of a very considerable effort, particularly in computational mechanics, and of competition with FEMs. Despite its undeniable success and remarkable advantages for some kinds of problems, collocation BEM is known to exhibit certain unpleasant features, among them the lack of symmetry which plays a key role in various theoretical developments and analysis procedures. The Symmetric Galerkin BEM (SGBEM) [4, 29] can be regarded as a response to the drawbacks of collocation BEM and it is recognized as particularly suitable for solving mixed boundary value problems and for coupling with FEM. Actually, nowadays, FEMs and BEMs are considered complementary rather that competitive. This feature is used in numerical strategies based on FEM-BEM coupling [6, 32], where some nonlinear or heterogeneous subregion is modeled by using finite elements, while the linear and homogeneous complementary domain is treated with boundary elements on the interface. Further, since the '80s, a great amount of literature has been produced on efficient evaluation of double boundary integrals with singular kernels involved in SGBEM (see e.g. [1, 2] and references therein).

On the other side, the new Isogeometric Analysis approach (IgA), introduced by Hughes et al. [14], establishes a strict relation between the geometry of the problem domain and the representation of the approximate solution, giving surprising computational advantages. It has also brought a renewed interest for BEMs, since one has to consider only a discretization of the domain boundary, which can be done in an accurate way by standard geometric modeling techniques, see e.g. [10, 11].

*Corresponding Author
Email addresses: alessandra.aimi@unipr.it (A. Aimi), mauro.diligenti@unipr.it (M. Diligenti), marialucia.sampoli@unisi.it (M. L. Sampoli), alessandra.sestini@unifi.it (A. Sestini)

Great part of IgA literature has been focused on FEMs and only recently the IgA approach has been introduced in the framework of BEMs, giving rise to the so-called IGA-BEM. Indeed, the first usage of IGA-BEM can be found in [22], where it is applied to exterior potential flow problems. Limiting here to a brief excursus in the literature related to the 2D case which is of interest in this paper, we mention that such approach has been later extended to problems with circulation [23]. In 2012 Simpson et al. developed an IGA-BEM in the elastostatic setting [28], showing its superiority with respect to the conventional BEM formulation. An application to structural optimization has been presented in [16]. However we note that all the mentioned works and most of the IGA-BEM formulations appeared in the literature rely on a discretization by collocation, thus producing a non symmetric coefficient matrix. In [3] for the first time a symmetric Galerkin formulation of IGA-BEM has been investigated in the context of interior and exterior 2D Laplace problems, and its performances have been compared to those of both a standard and a curvilinear SGBEM. Later the same idea has been explored in [21] for two–dimensional crack problems. The recent hybrid BEM FEM proposal, introduced in [20] to deal with elasticity problems and relying on the IGA paradigm, is also worth to mention. Actually, even if the considered approach is restricted to star–shaped domains, it has the attractive property of not requiring the knowledge of the fundamental solution associated with the differential operator.

In this paper, in order to enlarge the class of boundaries exactly representable in the isogeometric framework, we extend the analysis of IGA-SGBEM developed in [3] to the case of non polynomial spline spaces, taking into account either Non Uniform Rational B-Splines (NURBS) or generalized trigonometric and exponential B–spline spaces. We present numerical simulations for several test problems comparing the presented approach with the curvilinear SGBEM, where the boundary of the domain is exactly represented by a parametric curve while the approximate solution is obtained using Lagrangian basis, and with a standard (conventional) SGBEM, where the approximated boundary and solution are expressed in terms of Lagrangian basis. The comparison clearly shows that also the IGA-SGBEM approach based on non polynomial spline spaces is capable of producing accurate numerical solutions with less degrees of freedom.

2. Non Polynomial spline spaces

In this section we briefly recall the definition and basic properties of the two generalizations of B-splines considered in this paper.

Let $p \in \mathbb{N},\ p \geq 1$ be given and let us consider a sequence of knots in $[a, b]$

$$\Xi := \{\xi_1 \leq \xi_2 \leq \cdots \leq \xi_{n+p+1}\}, \quad n \in \mathbb{N},\ \ n > p \tag{1}$$

where we assume that the endpoints have multiplicity $p+1$, i.e. $a = \xi_1 = \cdots = \xi_{p+1} < \cdots < \xi_{n+1} = \cdots = \xi_{n+p+1} = b$. Classical B-splines of degree p can be defined iteratively by the Cox-de Boor algorithm, see for instance [9], with the characteristic function of the interval $[\xi_i, \xi_{i+1})$ as starting element. Here we prefer to consider the hat functions as starting elements and give an integral recurrence relation in order to stress the analogy with the construction of generalized B-splines (fractions with zero denominators are considered vanishing):

$$B^{(1)}_{i,\Xi}(t) := \begin{cases} \frac{t-\xi_i}{\xi_{i+1}-\xi_i} & \text{if } t \in [\xi_i, \xi_{i+1}) \\ \frac{\xi_{i+2}-t}{\xi_{i+2}-\xi_{i+1}} & \text{if } t \in [\xi_{i+1}, \xi_{i+2}) \\ 0 & \text{elsewhere} \end{cases} \tag{2}$$

$$B^{(p)}_{i,\Xi}(t) := \int_{-\infty}^{t} \delta^{(p-1)}_{i,\Xi} B^{(p-1)}_{i,\Xi}(s)\mathrm{d}s - \int_{-\infty}^{t} \delta^{(p-1)}_{i+1,\Xi} B^{(p-1)}_{i+1,\Xi}(s)\mathrm{d}s,\ \ p \geq 2, \quad \text{where} \quad \delta^{(p)}_{i,\Xi} := \frac{1}{\int_{-\infty}^{+\infty} B^{(p)}_{i,\Xi}(s)\mathrm{d}s}\,. \tag{3}$$

Now it is well known [9] that classical B-splines are piecewise polynomial functions, that is $B^{(p)}_{i,\Xi}(t) \in \mathbb{P}_p,\ t \in [\xi_r, \xi_{r+1})$, for all r, where

$$\mathbb{P}_p := \langle 1, t, \ldots, t^{p-2}, t^{p-1}, t^p \rangle, \tag{4}$$

denotes the space of algebraic polynomials of degree p. B-splines possess several fundamental properties as positivity, partition of unity, minimum support, (local) linear independence and smoothness easily described by means of the knot

multiplicity. Moreover, denoting by

$$\mathbb{S}_{\Xi}^{p} := \left\{ \sum_{j=1}^{n} c_j B_{j,\Xi}^{(p)},\ c_j \in \mathbb{R} \right\}, \tag{5}$$

the linear space spanned by the given B-splines, it is well known that this space has dimension equal to n, that is $\{B_{j,\Xi}^{(p)},\ j = 1, \ldots, n\}$ are linearly independent and form a basis for such a space.
Unfortunately, B-splines are not able to exactly describe conic sections which are shapes of salient interest in some engineering applications. This motivated the introduction of NURBS which are defined as follows, see e.g. [10],

$$R_{i,\Xi,W}^{(p)}(t) := \frac{w_i B_{i,\Xi}^{(p)}(t)}{\sum_{j=1}^{n} w_j B_{j,\Xi}^{(p)}(t)},\ \ i = 1, \ldots, n, \tag{6}$$

where $W := \{w_i \in \mathbb{R}^+,\ i = 1, \ldots, n\}$ is the set of positive weights. Due to the above construction, NURBS can be considered a generalization of B–splines inheriting from them important properties and with the additional benefit of making possible exact representation of conic sections. Thus, they have become the key ingredient in commercial CAD systems. On the other hand, the NURBS representation suffers from some drawbacks which nowdays are considered relevant in the CAD community. Indeed the additional parameters (*weights*) do not have an evident geometric meaning and their selection is often unclear. Moreover the rational model cannot encompass transcendental curves while many of them (helix, cycloid, ...) are of interest in applications. In addition, the NURBS parametrization of conic sections does not correspond to natural arc-length parametrization[1], so that unevenly spaced points correspond to uniform partitions in the parameter space. As a last remark, the behavior of NURBS with respect to differentiation and integration operations, which are crucial in differential problems applications, is particularly unpleasant because the derivative of a degree-p rational function is of degree $2p$ while its exact integration can be hard, possibly involving non rational forms. These undesirable geometric properties of NURBS have caused an active research in the last decades within the CAGD community, aimed to propose an alternative to the rational model. It turns out that some of the possible alternatives presented in the literature on this concern also possess interesting properties with respect to differentiation and integration operators, thus being also particularly attractive for isogeometric analysis.
To make the paper self contained, we devote the remainder of this section to summarize the definition and basic properties of generalized B-splines. Further details can be found for example in [17], Section 2. Both classical and generalized B–splines are piecewise functions whose smoothness at the knots can be prescribed by fixing the knot multiplicity but they have a different local form. Indeed the sections of B-splines of order p are polynomial, while those of generalized B-splines belong to the following extended spaces:

$$\mathbb{P}_{p}^{u_i,v_i} := \langle 1, t, \ldots, t^{p-2}, u_i(t), v_i(t) \rangle,\ t \in [\xi_i, \xi_{i+1}),\ i = 1, \ldots, n+p, \tag{7}$$

where u_i, v_i, are suitable smooth functions, see [8] and references quoted therein. The functions u_i and v_i can be selected in order to achieve the exact representation of salient profiles of interest and/or to obtain special features. Popular choices for spaces (7) are:

$$\mathbb{T}_{p,\alpha_i} := \langle 1, t, \ldots, t^{p-2}, \cos(\alpha_i t), \sin(\alpha_i t) \rangle, \quad 0 < \alpha_i(\xi_{i+1} - \xi_i) < \pi, \tag{8}$$

$$\mathbb{E}_{p,\alpha_i} := \langle 1, t, \ldots, t^{p-2}, \exp(\alpha_i t), \exp(-\alpha_i t) \rangle, \quad 0 < \alpha_i \in \mathbb{R}, \tag{9}$$

which lead to *trigonometric* and *exponential* splines respectively. We remark also that generalized splines associated with the local space defined in (9) are often referred to as *hyperbolic splines*, since $\mathbb{E}_{p,\alpha_i}$ coincides with the space $\langle 1, t, \ldots, t^{p-2}, \cosh(\alpha_i t), \sinh(\alpha_i t) \rangle$.
Trigonometric and exponential splines allow an exact representation of conic sections as well as of some transcendental curves (helix, cycloid, ...) and they are very attractive also from the geometrical point of view. Indeed they are able to provide parameterizations of conic sections much more related to the arc length than NURBS.

[1] Only straight lines have a rational representation w.r.t. arc-length, [12].

It is well known that B-spline–like functions with sections in spaces (8) and (9) can be constructed as in [15], [17], [30]. Although more general constructions can be obtained with less restrictive hypotheses, a neat theory of generalized B-splines can be presented assuming that $u_i, v_i \in C^{p-1}[\xi_i, \xi_{i+1}]$ and

$$\langle U_i(t), V_i(t)\rangle,\ t \in [\xi_i, \xi_{i+1}],\ \text{ is a Chebyshev space,} \qquad \text{with} \quad U_i := \frac{\mathrm{d}^{p-1}}{\mathrm{d}t^{p-1}} u_i,\ V_i := \frac{\mathrm{d}^{p-1}}{\mathrm{d}t^{p-1}} v_i, \tag{10}$$

i.e. any non zero element in the space has at most one zero in $[\xi_i, \xi_{i+1}]$. Under the assumption in (10), we have that there exists a unique element in $\langle U_i, V_i\rangle$ which takes the values 0 and 1 (1 and 0) at the endpoints of the interval $[\xi_i, \xi_{i+1}]$. Moreover, such an element has no other zeros in the interval, so it is positive in (ξ_i, ξ_{i+1}). Thus, without loss of generality we can assume

$$U_i(\xi_i) > 0,\ U_i(\xi_{i+1}) = 0, \qquad V_i(\xi_i) = 0,\ V_i(\xi_{i+1}) > 0.$$

Then, according to [15] (see also [19], [30] and references therein), generalized B-splines, $N_{i,p}$, can be defined by the following recurrence relations completely similar to the classical polynomial case

$$N^{(1)}_{i,\Xi}(t) := \begin{cases} \frac{V_i(t)}{V_i(\xi_{i+1})} & \text{if } t \in [\xi_i, \xi_{i+1}), \\ \frac{U_{i+1}(t)}{U_{i+1}(\xi_{i+1})} & \text{if } t \in [\xi_{i+1}, \xi_{i+2}), \\ 0 & \text{elsewhere} \end{cases} \tag{11}$$

$$N^{(p)}_{i,\Xi}(t) := \int_{-\infty}^{t} \delta_{i,p-1} N^{(p-1)}_{i,\Xi}(s)\mathrm{d}s - \int_{-\infty}^{t} \delta_{i+1,p-1} N^{(p-1)}_{i+1,\Xi}(s)\mathrm{d}s,\ \ p \geq 2, \quad \text{where} \quad \delta_{i,p} := \frac{1}{\int_{-\infty}^{+\infty} N^{(p)}_{i,\Xi}(s)\mathrm{d}s}. \tag{12}$$

Generalized B-splines possess all the desirable properties of classical polynomial B-splines, [9, 15]. We collect them in the following proposition:

Proposition 1. *Let $N^{(p)}_{i,\Xi}$, $i = 1, \ldots, n$ be generalized B-splines of degree $p \geq 2$ associated with the knot sequence (1). Then, the following properties hold:*

- *piecewise structure:* $N^{(p)}_{i,\Xi}(t) \in \mathbb{P}_p^{u_j, v_j}, t \in [\xi_i, \xi_{i+1})$
- *positivity:* $N^{(p)}_{i,\Xi}(t) \geq 0$,
- *partition of unity:* $\sum_{i=1}^{n} N^{(p)}_{i,\Xi}(t) \equiv 1,\ t \in [\xi_{p+1}, \xi_{n+1}),\ p > 1$,
- *compact support:* $N^{(p)}_{i,\Xi}(t) = 0,\ \ t \notin [\xi_i, \xi_{i+p+1}]$,
- *smoothness:* $N^{(p)}_{i,\Xi}(t)$ *is* $p - \rho_j$ *times continuously differentiable at* ξ_j, *being* ρ_j *the multiplicity of* ξ_j *in the knot sequence* $\{\xi_i, \ldots, \xi_{i+p+1}\}$,
- *derivative:* $(N^{(p)}_{i,\Xi})'(t) = \delta_{i,p-1} N^{(p-1)}_{i,\Xi}(t) - \delta_{i+1,p-1} N^{(p-1)}_{i+1,\Xi}(t)$,
- *local linear independence:* $N^{(p)}_{i-p,\Xi}(t), \ldots, N^{(p)}_{i-1,\Xi}(t), N^{(p)}_{i,\Xi}(t)$ *are linearly independent on* $[\xi_i, \xi_{i+1})$.

In addition, a knot insertion procedure is also available, [30], and spaces (7) support a degree-raising process. For a given degree p and a fixed knot sequence Ξ, GB-splines with section spaces as in (8) and (9) will be referred to as exponential and trigonometric B-splines of degree p, respectively denoted as $\mathbb{ES}^p_{\Xi,\boldsymbol{\alpha}}$ $\mathbb{TS}^p_{\Xi,\boldsymbol{\alpha}}$, while the space generated by classical (polynomial) B-splines of degree p will be called $\mathbb{S}^p_\Xi$ in the following. Here $\boldsymbol{\alpha} = \{\ldots, \alpha_i, \ldots\}$ stands for the sets of real parameters in (8) and (9). Regarding the approximation power of these spaces, we have the following result:

Theorem 1. *For fixed values of α_i, $i = 1, \ldots, n$, when $h = \max_{i=1,\ldots,n+p} (\xi_{i+1} - \xi_i)$ tends to zero, both the spaces $\mathbb{ES}^p_{\Xi,\boldsymbol{\alpha}}$ and $\mathbb{TS}^p_{\Xi,\boldsymbol{\alpha}}$ approach $\mathbb{S}^p_\Xi$. Consequently the approximation power of the three spline spaces is the same.*

Proof. From the Taylor expansion we have that the spaces (9) (8) approach $\mathbb{P}_p$, see [8]:

$$\mathbb{T}_{p,\alpha_i} =< 1, h, \ldots, h^{p-3}, \cos(\alpha_i h), \sin(\alpha_i h) >=< 1, h, \ldots, h^{p-3}, h^{p-2}, h^{p-1} > +O((\alpha_i h)^p),$$

$$\mathbb{E}_{p,\alpha_i} < 1, h, \ldots, h^{p-3}, \exp(\alpha_i h), \exp(-\alpha_i h) >=< 1, h, \ldots, h^{p-3}, h^{p-2}, h^{p-1} > +O((\alpha_i h)^p).$$

Hence, considering the analogy between the two recurrence integral relations in (3) and (12), the thesis is derived. ■

3. Isogeometric Symmetric Galerkin Boundary Element Method

Let $\Omega \subset \mathbb{R}^2$ be a bounded, simply connected, open domain with a (piecewise) smooth boundary $\Gamma := \partial\Omega = \{\mathbf{x} = (x_1, x_2) \in \mathbb{R}^2 | \, \mathbf{x} = \mathbf{C}(t),\ t \in [a, b]\}$, given by parametric representation on the interval $[a, b]$. Let us further suppose that $\Gamma = \bar{\Gamma}_1 \cup \bar{\Gamma}_2$, where Γ_1 and Γ_2 are open disjoint subsets of Γ and *meas* $(\Gamma_1) > 0$. We now consider, as a model, the mixed boundary value problem (BVP) for the Laplace equation:

given $u^* \in H^{1/2}(\Gamma_1)$ *and* $q^* \in H^{-1/2}(\Gamma_2)$*, find* $u \in H^1(\Omega)$ *such that*

$$\begin{cases} \Delta u = 0 & \text{in } \Omega\,, \\ u = u^* & \text{on } \Gamma_1\,, \\ \frac{\partial u}{\partial \mathbf{n}} = q^* & \text{on } \Gamma_2\,, \end{cases} \tag{13}$$

where $\frac{\partial}{\partial \mathbf{n}}$ denotes the derivative with respect to the outer normal $\mathbf{n}$ to Γ.
The symmetric boundary integral formulation of problem (13) is based on the use of the following weakly, strongly and hyper-singular boundary integral operators, whose properties are established in [7, 27, 31]:

$$\begin{aligned} Vq(\mathbf{x}) &:= \int_\Gamma U(\mathbf{x}, \mathbf{y})\, q(\mathbf{y}) \mathrm{d}\gamma_\mathbf{y}\,, & Ku(\mathbf{x}) &:= \int_\Gamma \frac{\partial U}{\partial \mathbf{n}_\mathbf{y}}(\mathbf{x}, \mathbf{y})\, u(\mathbf{y}) \mathrm{d}\gamma_\mathbf{y}\,, \\ K'q(\mathbf{x}) &:= \int_\Gamma \frac{\partial U}{\partial \mathbf{n}_\mathbf{x}}(\mathbf{x}, \mathbf{y})\, q(\mathbf{y}) \mathrm{d}\gamma_\mathbf{y}\,, & Du(\mathbf{x}) &:= \int_\Gamma \frac{\partial^2 U}{\partial \mathbf{n}_\mathbf{x} \partial \mathbf{n}_\mathbf{y}}(\mathbf{x}, \mathbf{y})\, u(\mathbf{y}) \mathrm{d}\gamma_\mathbf{y}\,, \end{aligned} \tag{14}$$

where $U(\mathbf{x}, \mathbf{y}) := -\frac{1}{2\pi} \ln \|\mathbf{y} - \mathbf{x}\|_2$ is the fundamental solution of the 2D Laplace operator and K' is the adjoint of K with respect to the natural duality $< \cdot, \cdot >$ between $H^{1/2}(\Gamma)$ and its dual $H^{-1/2}(\Gamma)$, which for sufficiently smooth functions coincides with the usual scalar product in $L^2(\Gamma)$. Then, following [7, 31], problem (13) can be written as a system of two Boundary Integral Equations (BIE) of the first kind in the unknowns q on Γ_1 and u on Γ_2, of the form

$$\begin{bmatrix} V_{11} & -K_{12} \\ -K'_{21} & D_{22} \end{bmatrix} \begin{bmatrix} q \\ u \end{bmatrix} = \begin{bmatrix} -V_{12} & \frac{1}{2}I + K_{11} \\ -\frac{1}{2}I + K'_{22} & -D_{21} \end{bmatrix} \begin{bmatrix} q^* \\ u^* \end{bmatrix}, \tag{15}$$

where the boundary integral operators subscripts $j\,k$ mean evaluation over Γ_j and integration over Γ_k.
System (15) will be solved in a weak sense, searching $q \in H^{-1/2}(\Gamma_1)$ and $u \in H_0^{1/2}(\Gamma_2)$. After having recovered the missing Cauchy data by solving, with obvious meaning of notation, the weak symmetric problem:

$$< \begin{bmatrix} V_{11} & -K_{12} \\ -K'_{21} & D_{22} \end{bmatrix} \begin{bmatrix} q \\ u \end{bmatrix}, \begin{bmatrix} p \\ v \end{bmatrix} >=< \begin{bmatrix} f_1 \\ f_2 \end{bmatrix}, \begin{bmatrix} p \\ v \end{bmatrix} >, \qquad \forall\, [p, v] \in H^{-1/2}(\Gamma_1) \times H_0^{1/2}(\Gamma_2)\,, \tag{16}$$

one can use the representation formula

$$u(\mathbf{x}) = \int_\Gamma U(\mathbf{x}, \mathbf{y})\, q(\mathbf{y}) \mathrm{d}\gamma_\mathbf{y} - \int_\Gamma \frac{\partial U}{\partial \mathbf{n}_\mathbf{y}}(\mathbf{x}, \mathbf{y})\, u(\mathbf{y}) \mathrm{d}\gamma_\mathbf{y}\,, \qquad \mathbf{x} \in \Omega\,, \tag{17}$$

to obtain the solution at any point of the domain.
Remark. If we have to deal with a Dirichlet BVP, i.e. $\Gamma \equiv \Gamma_1$, the systems (15) obviously reduces to the first equation alone, where the only unknown is $q(\mathbf{x})$, i.e. $Vq = f$. A similar boundary integral equation can be written for a Dirichlet problem exterior to an open arc in the plane (see e.g. [5]): in this case, the unknown is the jump of $q(\mathbf{x})$ across the arc Γ, i.e. $[q(\mathbf{x})]_\Gamma$.

For the SGBEM discretization phase, we consider a uniform partition of the parametrization interval $[a, b] = \bigcup_{\ell=1}^n I_\ell$, made up by n subintervals I_ℓ and governed by the decomposition parameter $h = \mathit{length}(I_\ell)$. This induces over Γ, using the parametric representation of the boundary, a mesh $\Gamma_h = \bigcup_{\ell=1}^n e_\ell$, constituted by curvilinear elements $e_\ell = \mathbf{C}(I_\ell)$. In a similar way, a finite dimensional subspace of piecewise polynomial functions can then be lifted on the boundary, starting from the introduced partition of $[a, b]$.
In the IGA-SGBEM, the very same NURBS or generalized B-spline basis used to represent the boundary Γ is used also as a basis for the functional approximation space. This approach will be compared with the curvilinear SGBEM, where

the boundary of the problem can be given by any explicitly defined parametric representation, but the approximation space is spanned by a Lagrangian basis defined over the decomposition of $[a, b]$, and with the standard SGBEM, where Γ is approximated by a polygonal boundary $\tilde{\Gamma}_h$, constituted by linear elements, each interpolating the endpoints of e_ℓ, $\ell = 1, \cdots, n$, and a local Lagrangian basis is lifted onto each straight element of $\tilde{\Gamma}_h$ from the reference element $[0, 1]$. Then, using suitable numerical integration schemes for the approximation of weakly, strongly and hypersingular double integrals in (16) (see [2]), one can write down the linear, symmetric, non singular system, where the vector unknowns q_h, u_h collect the coefficients with respect to the selected basis, which allow to finally obtain an approximate solution of the integral problem.
Regarding the pointwise convergence of the presented approach, we recall theoretical results given in [25, 26] for classical spline spaces. In particular, for a pure Dirichlet problem, we can state the following theorem.

Theorem 2. [25] *If Γ is sufficiently smooth and regularly parameterized, and a uniform partition of the parametrization interval is used, then, denoting with q_h the IGA-SGBEM approximation in $\mathbb{S}^p_\Xi$ of the analytical solution of the BIE $Vq = f$, there exists a constant c such that*

$$\|q - q_h\|_{L^\infty} \leq c\, h^{p+1} \|q\|_{W^{p+1,\infty}} , \tag{18}$$

provided that $q \in W^{p+1,\infty}(\Gamma)$.

In the next Section, we give numerical evidence of the same rate of convergence for $q_h \in \mathbb{TS}^p_{\Xi,\boldsymbol{\alpha}}$. This result can be justified by the power of approximation of the considered generalized spline spaces, which, owing to Theorem 1, coincides with that of $\mathbb{S}^p_\Xi$.

4. Numerical results

In this section we show the effectiveness of the proposed generalized GA-SGBEM by some experiments. In all the examples we compare our results with those obtained with both curvilinear and standard SGBEM, respectively denoted with C-SGBEM and S-SGBEM.
The first two benchmarks possess smooth solutions. The solution of Example 1 even belongs to the chosen approximation space, hence its accurate recovery does not require any refinement. This is not the case for the solution of Example 2 but its smoothness allows us to confirm the convergence behavior of the scheme stated in Theorem 2. On the other hand, the problems considered in Examples 3–4 possess less regular solutions and therefore the convergence rate of the approximation is slower.

Example 1. Let us consider a Dirichlet BVP for the Laplace equation exterior to the circular arc Γ given by the following parametric representation on the interval $[0, 1]$

$$\begin{cases} x_1 = \cos(\pi/2\,(2 - t)) + 1 \\ x_2 = \sin(\pi/2\,(2 - t)) \end{cases} \qquad 0 \leq t \leq 1\,. \tag{19}$$

This quarter of circumference can be expressed also by a quadratic NURBS related to the extended knot vector T and weights W

$$T = \begin{bmatrix} 0 & 0 & 0 & 1 & 1 & 1 \end{bmatrix}, \qquad W = \begin{bmatrix} 1 & \dfrac{1}{\sqrt{2}} & 1 \end{bmatrix} \tag{20}$$

and to control points Q_i, $i = 0, 1, 2$, whose coordinates are collected in the following matrix

$$\mathbf{Q} = \begin{bmatrix} 0 & 0 & 1 \\ 0 & 1 & 1 \end{bmatrix}. \tag{21}$$

The Dirichlet datum is given in such a way that the solution of the related boundary integral equation is explicitly known and reads $[q(\mathbf{x})]_\Gamma = x_2 =: \varphi(x_2)$.
In Table 1 a comparison is reported for different values of the discretization parameter h, which uniformly decomposes the parameter interval $[0, 1]$. We consider the isogeometric approach based on quadratic C^1 NURBS, C^0 quadratic

Lagrangian basis for C-SGBEM and L^2 quadratic Lagrangian basis on piecewise linear approximation $\tilde{\Gamma}_h$ of Γ_h for S-SGBEM. Together with degrees of freedom (DoF) and spectral condition numbers of the associated matrices, we show the relative errors

$$E_M = \|\varphi - \varphi_h\|_\infty / \|\varphi\|_\infty \,. \tag{22}$$

The symbol $'-'$ means that the simulation can be skipped since more than the single precision accuracy is already obtained without any subdivision of the parameter interval $[0, 1]$.

	NURBS IGA-SGBEM			C-SGBEM			S-SGBEM		
h	DoF	$cond.$	E_M	DoF	$cond.$	E_M	DoF	$cond.$	E_M
1	3	$3.99 \cdot 10$	$1.42 \cdot 10^{-8}$	3	$2.04 \cdot 10$	$2.73 \cdot 10^{-2}$	3	$2.18 \cdot 10$	$1.98 \cdot 10^{-1}$
1/2	4	–	–	5	$2.84 \cdot 10$	$5.57 \cdot 10^{-3}$	6	$5.36 \cdot 10$	$1.26 \cdot 10^{-1}$
1/4	6	–	–	9	$4.83 \cdot 10$	$8.42 \cdot 10^{-4}$	12	$1.23 \cdot 10^{2}$	$5.13 \cdot 10^{-2}$
1/8	10	–	–	17	$9.22 \cdot 10$	$1.11 \cdot 10^{-4}$	24	$2.58 \cdot 10^{2}$	$3.10 \cdot 10^{-2}$
1/16	18	–	–	33	$1.83 \cdot 10^{2}$	$1.40 \cdot 10^{-5}$	48	$5.21 \cdot 10^{2}$	$2.08 \cdot 10^{-2}$
1/32	36	–	–	65	$3.64 \cdot 10^{2}$	$1.76 \cdot 10^{-6}$	96	$1.05 \cdot 10^{3}$	$1.35 \cdot 10^{-2}$

Table 1: Example 1: comparison of quadratic NURBS IGA-SGBEM with quadratic C-SGBEM and S-SGBEM for different values of h.

Remark. The same results given by NURBS IGA-SGBEM could be obtained by using an IGA-SGBEM based on generalized trigonometric B-splines of degree 2 [17], which can represent exactly the curve Γ on the interval $[0, 1]$ through the same extended knot vector (20), the same control points (21) and fixing the tension parameter $\alpha = \pi/2$. In particular: $DoF = 3$, $cond. = 3.99\,10^1$ and $E_M = 1.75\,10^{-8}$. Moreover, as we have already pointed out in the Introduction, the collocation approach remains an interesting alternative to Galerkin schemes and it turns out that collocation with generalized B-splines works very well in the IGA context [18]. Hence, we give a comparison between results obtained by trigonometric B-splines based IGA-SGBEM with those coming from collocation IGA-BEM, where collocation is done at the Greville abscissae as in [28]: $DoF = 3$, $cond. = 6.66\,10^0$ and $E_M = 2.68\,10^{-8}$. In conclusion, exactly as in [3] for the comparison between classical B-Splines based IGA-SGBEM and collocation BEM, the Galerkin technique is slightly more accurate than the collocation one, while the matrix condition number of the latter is better, even if the symmetry property useful in the coupling with FEM [6, 32] is lost.

Example 2. In the second example we consider a potential problem interior to the ellipsis shown in Figure 1 (left), that can be described by quadratic trigonometric B-spline curve, $\mathbf{C}(t)$, $t \in [0, 4]$, related to the extended knot vector

$$T = [0,\ 0,\ 0,\ 1,\ 2,\ 3,\ 4,\ 4,\ 4]\,, \tag{23}$$

with tension parameters $\alpha_i = \frac{\pi}{2}$ for all i and control points Q_i, $i = 0 \ldots, 6$, whose coordinates are collected in the following matrix

$$\mathbf{Q} = \begin{bmatrix} 0.2 & 0.2 & -0.2 & -0.2 & 0.2 & 0.2 \\ 0 & 0.3 & 0.3 & -0.3 & -0.3 & 0 \end{bmatrix}. \tag{24}$$

The quadratic trigonometric B-spline basis employed is shown in Figure 1 (right).

The differential problem is equipped with Dirichlet boundary condition $u^*(\mathbf{x}) = -(x_1 + x_2)$; the solution $q(\mathbf{x})$, $\mathbf{x} = \mathbf{C}(t) = (C_1(t), C_2(t))$, of the related boundary integral equation is explicitly known and it reads $q(\mathbf{x}) = q(\mathbf{C}(t)) = (C_1'(t) - C_2'(t))/\|\mathbf{C}'(t)\|_2$.

The comparison reported in Table 2, for different values of the discretization parameter h, which uniformly decomposes the parameter interval $[0, 4]$, involves C^1 quadratic trigonometric B-splines for IGA-SGBEM, C^0 quadratic Lagrangian basis for C-SGBEM and L^2 quadratic Lagrangian basis on piecewise linear approximation $\tilde{\Gamma}_h$ of Γ_h for S-SGBEM. Together with degrees of freedom and spectral condition numbers of the associated matrices, we show the relative errors

$$E =: \|q - q_h\|_{L^2} / \|q\|_{L^2}\,, \tag{25}$$

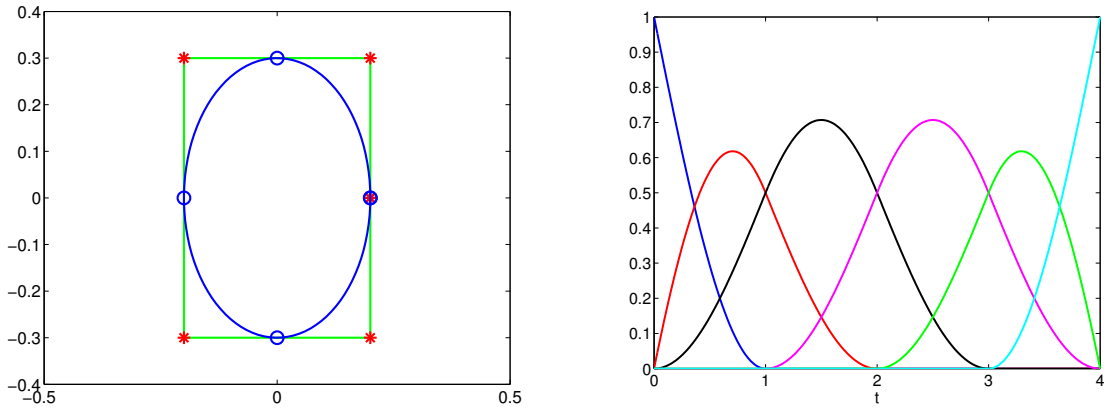

Figure 1: Example 2: the elliptic boundary, along with the related control polygon. The control points and the nodal (mesh) points of the curve are respectively marked with the symbol '$*$' and '$\circ$' (left); quadratic trigonometric B-spline basis related to (23) and $\alpha_i = \frac{\pi}{2}, \forall i$ (right).

in L^2 norm, which is the standard for the field q in boundary element analysis. These errors are also displayed in Figure 2 (left). The remarkable shape reproduction capability of the IGA-SGBEM approach based on quadratic trigonometric B-splines is underlined in Figure 2 (right) which shows the approximate solution obtained using $h = 1/16$ together with the analytical one.

Since the boundary of this example can be exactly defined also by using quadratic NURBS related to the extended

	$\mathbb{TS}^2$ IGA-SGBEM			C-SGBEM			S-SGBEM		
h	*DoF*	*cond.*	E	*DoF*	*cond.*	E	*DoF*	*cond.*	E
1	5	$5.37 \cdot 10$	$9.61 \cdot 10^{-2}$	8	$4.36 \cdot 10$	$4.93 \cdot 10^{-2}$	12	$6.36 \cdot 10$	$3.37 \cdot 10^{-1}$
1/2	9	$1.02 \cdot 10^{2}$	$2.33 \cdot 10^{-2}$	16	$9.07 \cdot 10$	$8.79 \cdot 10^{-3}$	24	$1.18 \cdot 10^{2}$	$9.90 \cdot 10^{-2}$
1/4	17	$2.07 \cdot 10^{2}$	$2.09 \cdot 10^{-3}$	32	$2.05 \cdot 10^{2}$	$1.16 \cdot 10^{-3}$	48	$2.56 \cdot 10^{2}$	$2.67 \cdot 10^{-2}$
1/8	33	$4.12 \cdot 10^{2}$	$1.61 \cdot 10^{-4}$	64	$4.62 \cdot 10^{2}$	$1.13 \cdot 10^{-4}$	96	$5.50 \cdot 10^{2}$	$6.74 \cdot 10^{-3}$
1/16	65	$9.33 \cdot 10^{2}$	$1.76 \cdot 10^{-5}$	128	$9.89 \cdot 10^{2}$	$8.70 \cdot 10^{-6}$	192	$1.15 \cdot 10^{3}$	$1.68 \cdot 10^{-3}$

Table 2: Example 2: comparison of results obtained by IGA-SGBEM (C^1 quadratic trigonometric B-splines) with those obtained by C-SGBEM (C^0 quadratic lagrangian basis) and S-SGBEM (L^2 quadratic lagrangian basis on $\tilde{\Gamma}_h$), for different for different values of the parameter h.

	NURBS IGA-SGBEM		
h	DoF	cond.	E
1	8	$2.82\,10^{2}$	$2.94\,10^{-2}$
1/2	12	$1.79\,10^{2}$	$8.92\,10^{-3}$
1/4	20	$2.93\,10^{2}$	$1.60\,10^{-3}$
1/8	36	$6.93\,10^{2}$	$1.53\,10^{-4}$
1/16	68	$1.63\,10^{3}$	$1.70\,10^{-5}$

Table 3: Example 2: quadratic NURBS based IGA-SGBEM results, for different values of the parameter h.

knot vector

$$T = [0,\ 0,\ 0,\ 1,\ 1,\ 2,\ 2,\ 3,\ 3,\ 4,\ 4,\ 4]\,, \tag{26}$$

with the following weights and control points,

$$W = \left[1 \quad \frac{1}{\sqrt{2}} \quad 1 \quad \frac{1}{\sqrt{2}} \quad 1 \quad \frac{1}{\sqrt{2}} \quad 1 \quad \frac{1}{\sqrt{2}} \quad 1\right] \tag{27}$$

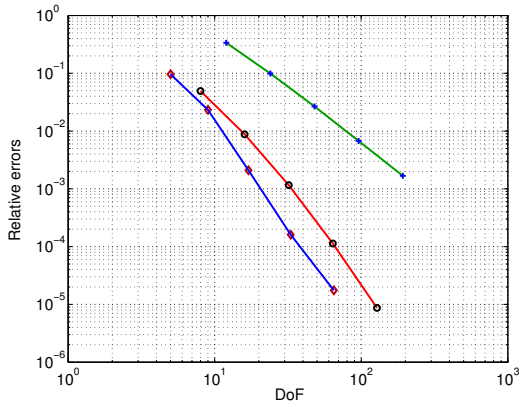

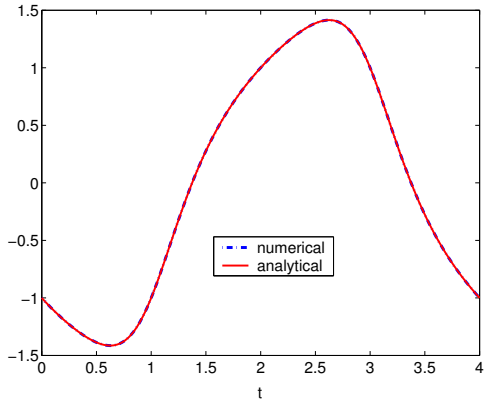

Figure 2: Example 2: relative errors of Table 2 vs DoF ('$\diamond$' trigonometric B-spline basis, '$\circ$' Lagrangian basis, + Lagrangian basis on $\tilde{\Gamma}_h$) (left); approximate solution obtained with $\mathbb{TS}^2$ IGA-SGBEM and $h = 1/16$, together with the analytical solution (right).

$$\mathbf{Q} = \begin{bmatrix} 0.2 & 0.2 & 0 & -0.2 & -0.2 & -0.2 & 0 & 0.2 & 0.2 \\ 0 & 0.3 & 0.3 & 0.3 & 0 & -0.3 & -0.3 & -0.3 & 0 \end{bmatrix}, \tag{28}$$

we give in Table 3 results obtained by the NURBS based IGA-SGBEM.
For this example, we give also in Table 4 the rate of convergence of quadratic trigonometric B-spline and of quadratic NURBS based IGA-SGBEM, referred to the error E_M defined in (22), showing that the experiments are in accordance with the theoretical expectations. Furthermore, the last row of the table shows the ratio between the elapsed time in the generation of the final linear system matrix operated by trigonometric B-splines and NURBS. Such ratio clearly indicates that, when possible, the use of generalized B-splines is preferable, because it gives the same accuracy of NURBS, but better performance in terms of computational cost, also avoiding the need of weights.

h	1	1/2	1/4	1/8	1/16
$\mathbb{TS}^2$ IGA-SGBEM					
$E_M(h)$	$1.37 \cdot 10^{-1}$	$3.28 \cdot 10^{-2}$	$4.39 \cdot 10^{-3}$	$3.73 \cdot 10^{-4}$	$4.03 \cdot 10^{-5}$
$\log_2\left(\frac{E_M(2h)}{E_M(h)}\right)$	–	2.06	2.90	3.56	3.21
NURBS IGA-SGBEM					
$E_M(h)$	$4.89 \cdot 10^{-2}$	$2.53 \cdot 10^{-2}$	$2.87 \cdot 10^{-3}$	$2.88 \cdot 10^{-4}$	$3.54 \cdot 10^{-5}$
$\log_2\left(\frac{E_M(2h)}{E_M(h)}\right)$	–	0.95	3.14	3.32	3.02
$\text{Time}_{\mathbb{TS}^2}/\text{Time}_{NURBS}$	$2.78 \cdot 10^{-2}$	$1.65 \cdot 10^{-2}$	$1.29 \cdot 10^{-2}$	$1.17 \cdot 10^{-2}$	$9.99 \cdot 10^{-3}$

Table 4: Example 2: Convergence orders of $\mathbb{TS}^2$ (up) and NURBS (down) IGA-SGBEM, varying h. In the last row the ratios between the corresponding computational times

At last, since one of the major strengths of BEM approach (with respect to FEM) is its ability of easily treating domains with holes, let us now consider the trimmed domain depicted in Figure 3, whose boundary curves are represented by quadratic trigonometric B-splines, each related to the extended knot vector (23), with tension parameters $\alpha_i = \frac{\pi}{2}$, for all i, and to control points collected in the following matrices

$$Q_{\text{est}} = \begin{bmatrix} 0.4 & 0.4 & -0.4 & -0.4 & 0.4 & 0.4 \\ 0 & 0.6 & 0.6 & -0.6 & -0.6 & 0 \end{bmatrix}, \quad Q_{\text{int}} = \begin{bmatrix} 0.1 & 0.1 & -0.3 & -0.3 & 0.1 & 0.1 \\ 0.2 & 0.5 & 0.5 & -0.1 & -0.1 & 0.2 \end{bmatrix}. \tag{29}$$

Here a mixed BVP is considered, where a Dirichlet condition $u^*(\mathbf{x}) = 1$ is assigned on the interior boundary, while a Neumann condition $q^*(\mathbf{x}) = 0$ is prescribed on the exterior boundary. This configuration can model a stationary heat

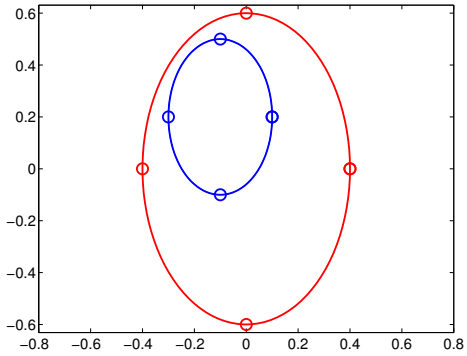

Figure 3: Example 2: the trimmed domain with elliptic boundaries. The nodal (mesh) points on the curves are marked with the symbol '$\circ$'.

conduction problem, where a constant temperature on the inner wall and a zero heat flux on the outer wall are given. We have tested our IGA-SGBEM approach just using the quadratic trigonometric spline space $\mathbb{TS}^2$ used to define the boundary curves. The resulting linear system is of order 10 and the approach produces an approximate solution with an absolute error in maximum norm equal to $4.6956\,10^{-4}$ for what concerns the recovered flux q and equal to $2.4261\,10^{-4}$ for what concerns the recovered potential u. If we use quadratic Lagrangian basis for C-SGBEM, instead, we have to solve a liner system of order 16 to reproduce the same error order.
Note that the obtained errors are due only to the approximation, at a fixed accuracy, of hypersingular double boundary integrals. Such integrals, arising in the IGA-SGBEM resolution of this mixed BVP, are approximated by the quadrature formulas introduced in [2].

Example 3. In the third example we consider a potential problem interior to the free-form domain shown in Figure 4 (left), similar to the one considered in [23]. Such a domain has a smooth boundary that can be described by a closed rational B-spline curve of degree 3, $\mathbf{C}(t)$, $t \in [0, 1]$, with uniform breakpoints and mesh step $h = 1/8$. Indeed, the curve has been obtained by taking the same control polygon of [3], Example 2, and modifying the weights. The

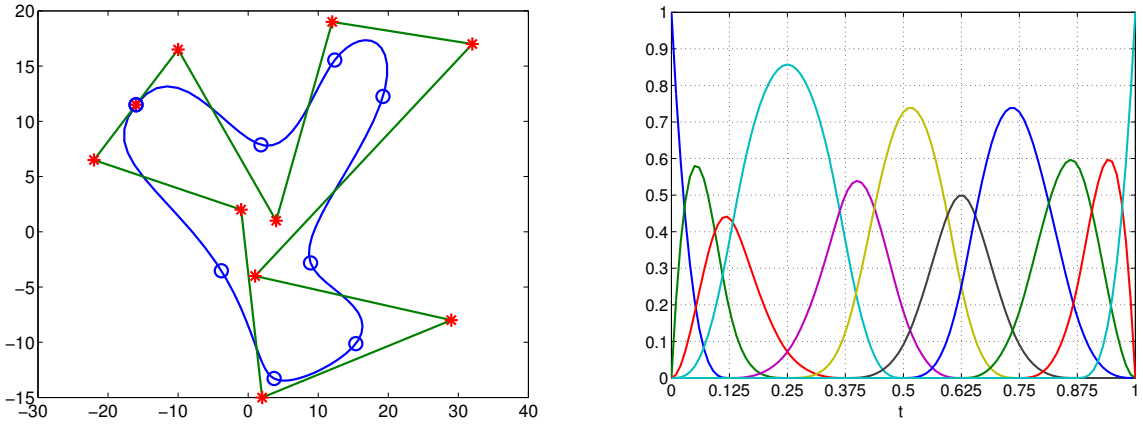

Figure 4: Example 3: the cubic closed NURBS curve defining the boundary of the considered interior domain along with its control polygon. The control points and the nodal (mesh) points of the NURBS curve are respectively marked with the symbol '$*$' and '$\circ$' (left); NURBS basis of degree 3 related to (30)–(31) (right).

corresponding basis is shown in Figure 4 (right), related to the extended knot vector

$$T = [0,\ 0,\ 0,\ 0,\ 0.125,\ 0.25,\ 0.375,\ 0.5, 0.625,\ 0.75,\ 0.875,\ 1,\ 1,\ 1,\ 1]\,, \tag{30}$$

with weights

$$W = \begin{bmatrix} 1 & 1 & 1 & 3 & 1 & 1 & 0.5 & 1 & 1 & 1 & 1 \end{bmatrix} \tag{31}$$

and to control points Q_i, $i = 0\ldots, 10$, whose coordinates are collected in the following matrix

$$\mathbf{Q} = \begin{bmatrix} -16 & -22 & -1 & 2 & 29 & 1 & 32 & 12 & 4 & -10 & -16 \\ 11.5 & 6.5 & 2 & -15 & -8 & -4 & 17 & 19 & 1 & 16.5 & 11.5 \end{bmatrix}.$$

The differential problem is equipped with Dirichlet boundary condition $u^*(\mathbf{x}) = -(x_1 + x_2)$; as in the previous example, the solution $q(\mathbf{x})$, $\mathbf{x} = \mathbf{C}(t)$, of the related boundary integral equation is explicitly known, it reads $q(\mathbf{x}) = q(\mathbf{C}(t)) = (C_1'(t) - C_2'(t))/\|\mathbf{C}'(t)\|_2$ and, as function of t, now it is C^1 regular on $[0, 1]$.

At first, in order to put in evidence possible benefits of our approach, we fix the degree of the piecewise polynomial

	NURBS IGA-SGBEM			C-SGBEM			S-SGBEM		
h	*DoF*	*cond.*	E_M	*DoF*	*cond.*	E_M	*DoF*	*cond.*	E_M
1/8	10	$8.59 \cdot 10^2$	$3.27 \cdot 10^{-1}$	24	$6.03 \cdot 10^2$	$5.48 \cdot 10^{-2}$	32	$4.02 \cdot 10^2$	$4.41 \cdot 10^{-1}$
1/16	18	$1.15 \cdot 10^3$	$1.04 \cdot 10^{-1}$	48	$1.56 \cdot 10^3$	$2.21 \cdot 10^{-2}$	64	$1.02 \cdot 10^3$	$4.74 \cdot 10^{-1}$
1/32	34	$2.73 \cdot 10^3$	$1.52 \cdot 10^{-2}$	96	$4.15 \cdot 10^3$	$2.86 \cdot 10^{-3}$	128	$3.12 \cdot 10^3$	$1.04 \cdot 10^{-1}$
1/64	66	$9.39 \cdot 10^3$	$2.52 \cdot 10^{-3}$	192	$1.02 \cdot 10^4$	$1.37 \cdot 10^{-4}$	256	$7.46 \cdot 10^3$	$2.47 \cdot 10^{-2}$

Table 5: Example 3: comparison of results obtained by C^2 cubic NURBS (left) with those obtained by C^0 cubic Lagrangian basis (middle) and by L^2 cubic Lagrangian basis on $\tilde{\Gamma}_h$ (right).

spaces equal to 3 and compare the results obtained by using C^2 NURBS in IGA-SGBEM and C^0 Lagrangian basis in C-SGBEM. The comparison is done in Table 5: for each considered mesh size h, the corresponding total number of degrees of freedom, the spectral condition number of the discretization matrix, and relative errors E, defined in (25), are given. We note that the errors with the IGA-SGBEM approach are worse, but the number of degrees of

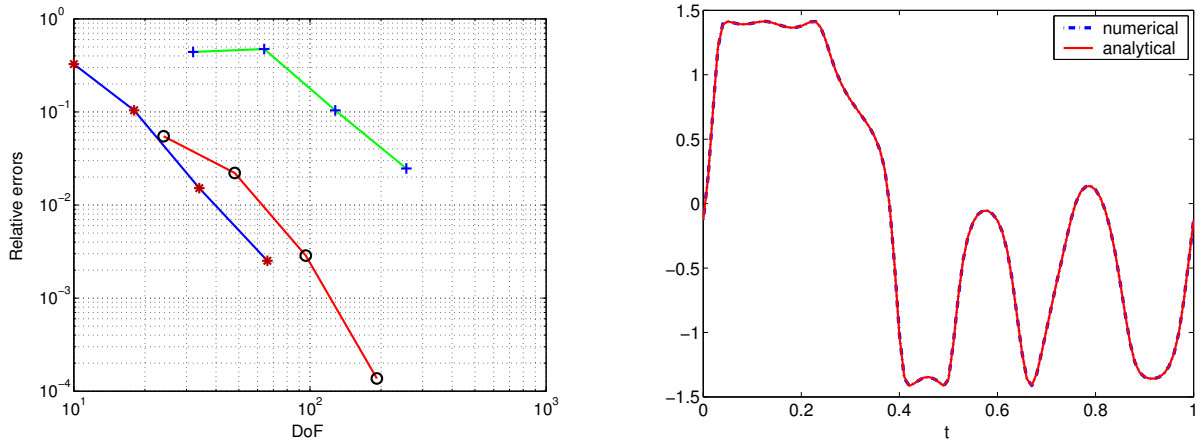

Figure 5: Example 3: relative errors of Table 5 vs DoF ('$*$' NURBS basis, '$\circ$' Lagrangian basis, + Lagrangian basis on $\tilde{\Gamma}_h$) (left); approximate solution obtained with NURBS basis of degree 3 and $h = 1/64$, together with the analytical solution (right).

freedom is remarkably lower. To complete this benchmark, on the right of Table 5, for the same values of h, results obtained using L^2 cubic Lagrangian basis on piecewise linear approximation $\tilde{\Gamma}_h$ of the boundary Γ are reported. All the error behaviors are shown in Figure 5 (left) with respect to degrees of freedom: we can observe that the decay of the errors coming from IGA-SGBEM approach and C-SGBEM has the same slope, but in IGA-SGBEM results are obtained using a lower number of degrees of freedom, while S-SGBEM gives poor results due to the error in the approximation of the boundary. At last, the approximate solution obtained using $h = 1/64$ and cubic NURBS perfectly matching the analytical solution is shown in Figure 5 (right). For this example, we further present a comparison of the results obtained working in nested C^2 spaces of increasing degree ≥ 3, spanned by NURBS bases (IGA-SGBEM), with those obtained working with larger C^0 spline spaces of corresponding degree spanned by the Lagrangian basis (C-SGBEM). Note that the boundary curve is exactly expressed in all the simulations, and its representation can be

$h = 1/8$	NURBS IGA-SGBEM			C-SGBEM		
degree	*DoF*	*cond.*	E	*DoF*	*cond.*	E
3	10	$8.59 \cdot 10^{2}$	$3.27 \cdot 10^{-1}$	24	$6.03 \cdot 10^{2}$	$5.48 \cdot 10^{-2}$
4	18	$4.25 \cdot 10^{3}$	$1.03 \cdot 10^{-1}$	32	$1.24 \cdot 10^{3}$	$5.22 \cdot 10^{-2}$
5	26	$1.90 \cdot 10^{4}$	$4.32 \cdot 10^{-2}$	40	$1.92 \cdot 10^{3}$	$2.27 \cdot 10^{-2}$
6	34	$9.10 \cdot 10^{4}$	$1.90 \cdot 10^{-2}$	48	$3.98 \cdot 10^{3}$	$1.31 \cdot 10^{-2}$
7	42	$4.37 \cdot 10^{5}$	$1.34 \cdot 10^{-2}$	56	$4.73 \cdot 10^{3}$	$1.15 \cdot 10^{-2}$
8	50	$2.12 \cdot 10^{6}$	$8.84 \cdot 10^{-3}$	64	$1.57 \cdot 10^{4}$	$9.78 \cdot 10^{-3}$
9	58	$1.03 \cdot 10^{7}$	$4.68 \cdot 10^{-3}$	72	$1.23 \cdot 10^{4}$	$4.28 \cdot 10^{-3}$
$h = 1/16$	NURBS IGA-SGBEM			C-SGBEM		
degree	*DoF*	*cond.*	E	*DoF*	*cond.*	E
3	18	$1.15 \cdot 10^{3}$	$1.04 \cdot 10^{-1}$	48	$1.56 \cdot 10^{3}$	$2.21 \cdot 10^{-2}$
4	34	$8.35 \cdot 10^{3}$	$1.91 \cdot 10^{-2}$	64	$3.14 \cdot 10^{3}$	$8.00 \cdot 10^{-3}$
5	50	$4.15 \cdot 10^{4}$	$9.07 \cdot 10^{-3}$	80	$4.56 \cdot 10^{3}$	$5.05 \cdot 10^{-3}$
6	66	$2.19 \cdot 10^{5}$	$3.59 \cdot 10^{-3}$	96	$9.38 \cdot 10^{3}$	$1.94 \cdot 10^{-3}$
7	82	$1.16 \cdot 10^{6}$	$1.97 \cdot 10^{-3}$	112	$1.04 \cdot 10^{4}$	$1.48 \cdot 10^{-3}$
8	98	$6.13 \cdot 10^{6}$	$1.13 \cdot 10^{-3}$	128	$3.71 \cdot 10^{4}$	$7.26 \cdot 10^{-4}$
9	114	$3.15 \cdot 10^{7}$	$2.92 \cdot 10^{-4}$	144	$2.55 \cdot 10^{4}$	$3.22 \cdot 10^{-4}$

Table 6: Example 3: comparison between results obtained with IGA-SGBEM based on C^2 NURBS and C-SGBEM based on C^0 Lagrangian basis, for different degrees of the piecewise polynomial basis and for $h = 1/8,\ 1/16$.

obtained combining a *degree elevation* procedure with a *knot insertion* procedure (see e.g. [10]). Results are presented in Table 6, for fixed $h = 1/8,\ 1/16$ and for the considered increasing degrees. The relative errors (25) are then plotted in Figure 6 with respect to degrees of freedom. Let us note that the IGA-SGBEM approach is slightly superior to C-SGBEM which employs Lagrangian basis, giving the same error order but using less degrees of freedom, even if in these simulations the conditioning of NURBS systems are worse than the corresponding Lagrangian ones.

Example 4. In this example we consider a potential problem interior to the domain shown in Figure 7 (left), which has four sharp corners. The boundary of the domain is described by a closed parametric piecewise exponential curve, $\mathbf{C}(t)$, $t \in [0, 4]$. Such curve can be represented by a quadratic exponential B-spline (see Figure 7 (right)) associated to the following extended knot vector

$$T = [0,\ 0,\ 0,\ \tfrac{1}{6}\!:\!\tfrac{1}{6}\!:\!\tfrac{5}{6},\ 1,\ 1,\ \tfrac{7}{6}\!:\!\tfrac{1}{6}\!:\!\tfrac{11}{6},\ 2,\ 2,\ \tfrac{13}{6}\!:\!\tfrac{1}{6}\!:\!\tfrac{17}{6},\ 3, 3,\ \tfrac{19}{6}\!:\!\tfrac{1}{6}\!:\!\tfrac{23}{6},\ 4,\ 4,\ 4]\,, \tag{32}$$

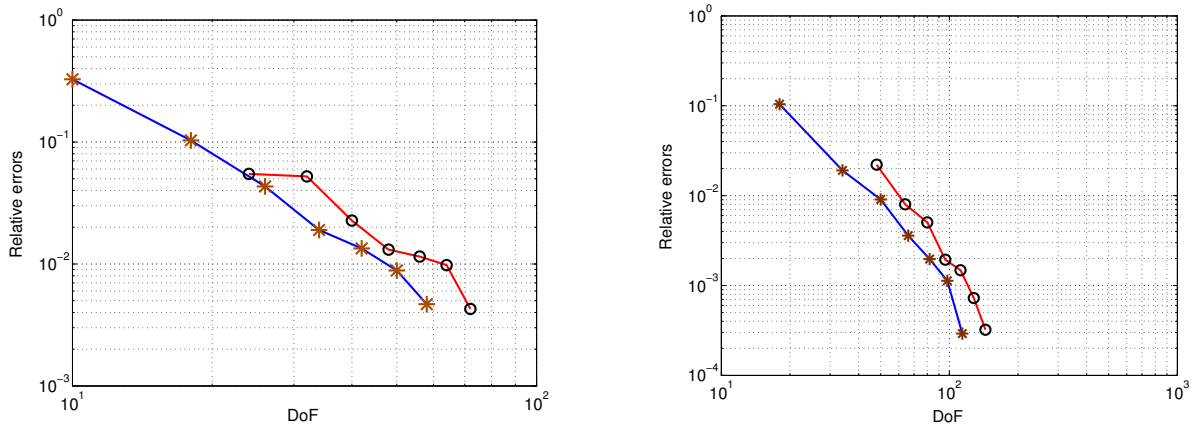

Figure 6: Example 3: relative errors of Table 6 vs DoF with $h = 1/8$ (left) and $h = 1/16$ (right) ($'*'$ NURBS basis, $'\circ'$ Lagrangian basis).

and to control points $\mathbf{Q}_i$, $i = 0, \ldots, 28$, shown by stars in Figure 7 (left). The tension parameters are $\alpha_i = 2$ for all i. Considering that (32) is an open knot vector and the breakpoints $1, 2, 3$ specified in (32) have double multiplicity, it turns out that $\mathbf{C}(t) \in C^0([0, 4])$. In this way, the geometry of the domain boundary can be exactly described and constitutes a challenging benchmark for BEMs, due to the presence of four sharp corners. The differential problem is

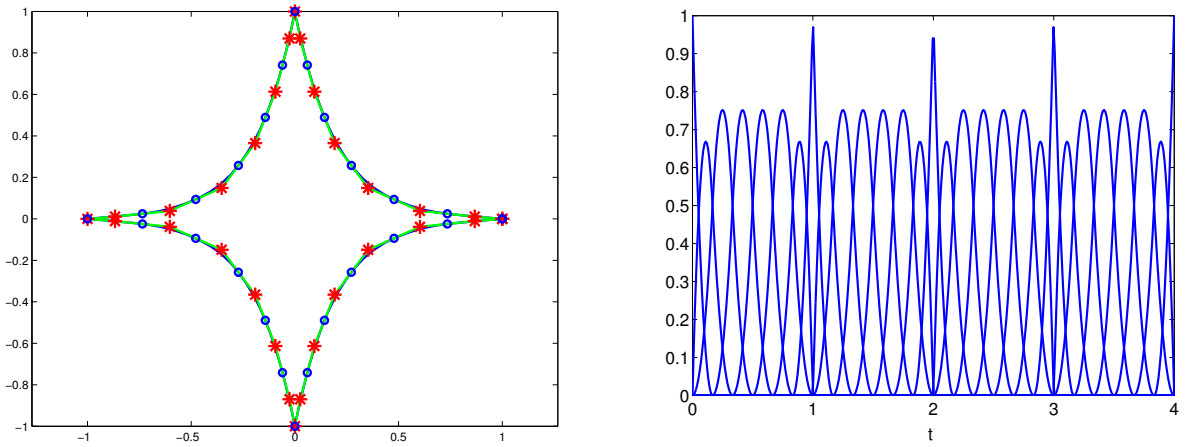

Figure 7: Example 4: the considered boundary, along with the related control polygon. The control points and the nodal (mesh) points of the curve are respectively marked with the symbol '$*$' and '$\circ$' (left); quadratic exponential B-spline basis related to (32) and $\alpha_i = 2, \forall i$ (right).

equipped with Dirichlet boundary condition $u^*(\mathbf{x}) = -(x_1 + x_2)$; as in the previous example, the solution $q(\mathbf{x})$, $\mathbf{x} = \mathbf{C}(t)$, of the related boundary integral equation is explicitly known, it reads $q(\mathbf{x}) = q(\mathbf{C}(t)) = (C_1'(t) - C_2'(t))/\|\mathbf{C}'(t)\|_2$, but now, as function of t, it belongs to $L^2(0, 4)$ and presents finite jumps for $t = 1, 2, 3$.
As a first choice, we do not care about the low regularity of the solution and we work in the space used to describe the boundary which is spanned by the quadratic exponential B-splines associated to (32) and is a subset of $C^0[0, 4]$. Then we successively extend the space by inserting a new simple knot at the midpoint between any two successive breakpoints (this corresponds to halving the mesh step h, since uniform distributions of the breakpoints are always assumed).

h	DoF	$cond.$	E
$1/6$	28	$9.62 \cdot 10^2$	$2.38 \cdot 10^{-1}$
$1/12$	52	$2.06 \cdot 10^3$	$1.60 \cdot 10^{-1}$
$1/24$	100	$4.23 \cdot 10^3$	$1.06 \cdot 10^{-1}$

Table 7: Example 4: results obtained by C^0 quadratic generalized exponential B-splines starting from extended knot vector (32).

In Table 7, the obtained results are shown: for each considered h, the corresponding total number of degrees of freedom, the spectral condition number of the IGA-SGBEM discretization matrix and the relative error (25) are given. Figure 8 confirms that the numerical solution obtained with $h = 1/24$ mainly agrees with the analytical one. As expected, the jumps are smoothly approximated; small oscillations occur in the neighborhood of these jumps, due to the steep layers of the continuous approximate solution. In order to adequate the quadratic exponential spline space to the low regularity of the analytical solution, we have then performed a similar set of experiments starting now from the extended knot vector (32), where the multiplicity of breakpoints $1, 2, 3$ has been augmented by one unit.
In Table 8, we show the comparison between the results obtained successively refining the parameter h for the $L^2(0, 4)$ quadratic generalized exponential B-splines in IGA-SGBEM, the $L^2(0, 4)$ quadratic Lagrangian basis in C-SGBEM and L^2 quadratic Lagrangian basis on piecewise linear approximation $\tilde{\Gamma}_h$ of Γ for S-SGBEM. In particular, for all the approaches, we present the total number of degrees of freedom, the spectral condition number of the associated linear system matrix and the relative error (25).

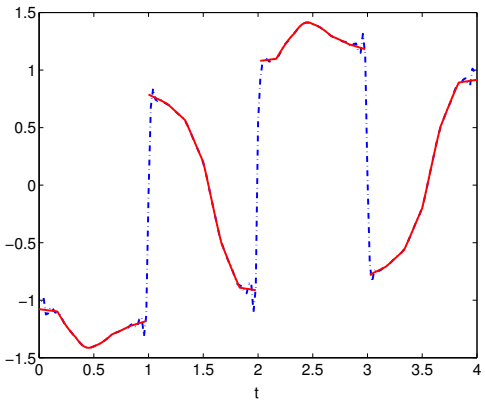

Figure 8: Example 4: the analytical solution (solid) and the continuous numerical solution (dash-dotted), obtained after two refinements ($h = 1/24$).

	$\mathbb{ES}^2$ IGA-SBEM			C-SGBEM			S-SGBEM		
h	*DoF*	*cond.*	E	*DoF*	*cond.*	E	*DoF*	*cond.*	E
1/6	32	$1.11 \cdot 10^3$	$5.94 \cdot 10^{-2}$	52	$1.09 \cdot 10^3$	$3.60 \cdot 10^{-1}$	72	$2.61 \cdot 10^2$	$5.05 \cdot 10^{-1}$
1/12	56	$2.38 \cdot 10^3$	$5.46 \cdot 10^{-2}$	100	$2.25 \cdot 10^3$	$2.49 \cdot 10^{-1}$	144	$5.51 \cdot 10^2$	$3.52 \cdot 10^{-1}$
1/24	104	$4.89 \cdot 10^3$	$4.27 \cdot 10^{-2}$	196	$4.54 \cdot 10^3$	$1.78 \cdot 10^{-1}$	288	$1.13 \cdot 10^3$	$2.48 \cdot 10^{-1}$

Table 8: Example 4: comparison of $\mathbb{ES}^2$ IGA-SGBEM with quadratic C-SGBEM and S-SGBEM, all based on $L^2(0,4)$ basis functions, for different values of h.

Figure 9 (right) shows the $L^2(0,4)$ IGA-SGBEM numerical solution obtained with $h = 1/24$ together the analytical one. At last, errors of Table 8 are reported in Figure 9 (left) which confirms that even in this case the best results are obtained with the IGA-SGBEM approach. Note that the rate of convergence of all the considered schemes is rather low due to the lack of regularity of the solution.

5. Conclusions

In this paper, extending the investigation made in [3] for classical B-splines, the behavior of IGA-SGBEM based on both NURBS and generalized B-splines is analyzed. We recall that the IGA paradigm uses the same representation to define either the geometry of the boundary domain and the approximate solution of the problem. In the present work this idea is applied to a symmetric Galerking BEM and the proposed new formulations of the scheme are compared to classical SGBEM, both standard and curvilinear. Results confirm that, in terms of accuracy per degrees of freedom, isogeometric SGBEM performs better than curvilinear SGBEM and much better than standard SGBEM, which of course introduces an approximation of the boundary, too. When possible, i.e. when the boundary is exactly representable by both NURBS and generalized B-splines, a comparison between them has been pointed out too. It reveals the same performance in terms of accuracy, but the superiority of generalized B-splines on NURBS for what concerns the computational cost. Anyway, a key point for improving the elapsed time for the IGA-SGBEM techniques is that of abandoning an element-by-element assembly strategy, suitable for Lagrangian basis, by introducing quadrature formulas tailored on the new basis. The aim is to obtain a still accurate but more efficient treatment of double boundary integrals with kernel singularities which can also allow a different assembly organization. This is the topic of our ongoing research.

Acknowledgements

This work has been partially supported by INdAM, through GNCS research projects.

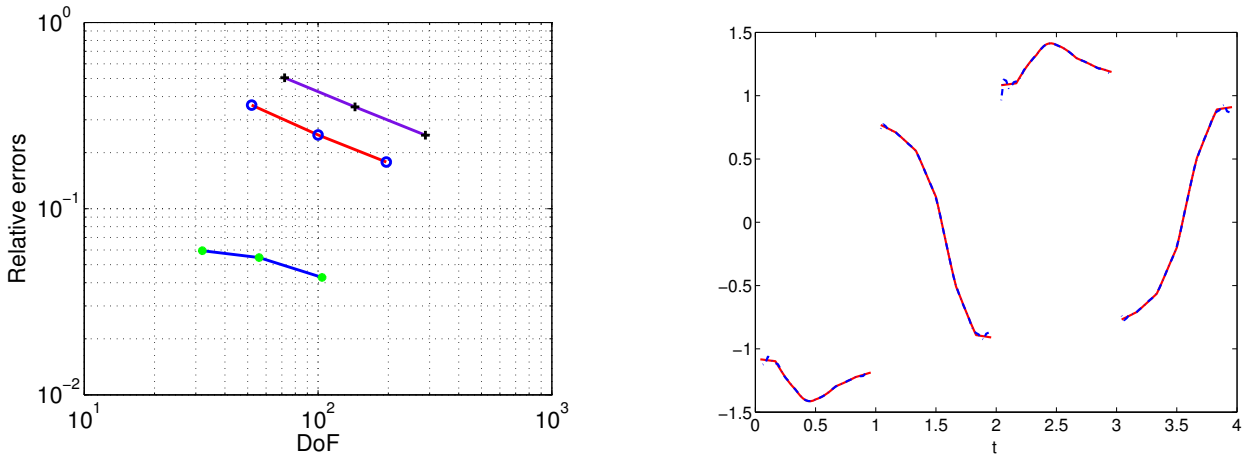

Figure 9: Example 4: relative errors of Table 8 vs DoF ($'*'$ $\mathbb{ES}^2$ basis, $'\circ'$ Lagrangian basis, + Lagrangian basis on $\tilde{\Gamma}_h$) (left); the analytical solution (solid) and the $L^2(0,4)$ IGA-SGBEM numerical solution (dash-dotted), obtained with $h = 1/24$ (right).

[1] A. Aimi, M. Diligenti, G. Monegato; New numerical integration schemes for applications of Galekin BEM to 2D problems, *Internat. J. Numer. Methods Engrg.*, **40**, 1977–1999, (1997).

[2] A. Aimi, M. Diligenti, G. Monegato; Numerical integration schemes for the BEM solution of hyoersingular integral equations, *Internat. J. Numer. Methods Engrg.*, **45**, 1807–1830, (1999).

[3] A. Aimi, M. Diligenti, M. L. Sampoli, A. Sestini; Isogeometric Analysis and Symmetric Galerkin BEM: a 2D numerical study, *Applied Math. and Comp.*, **272**, 173-186, (2016).

[4] M. Bonnet, G. Maier, C. Polizzotto, Symmetric Galerkin boundary element method, *Appl. Mech. Rev.*, **5**1, 669–704, (1998).

[5] G. Chen, J. Zhou; Boundary Element Methods, Computational Mathematics and Applications, Academic Press, London, (1992).

[6] M. Costabel, Symmetric Methods for the coupling of Finite Elements and Boundary elements, in: C.A. Brebbia, W.L. Wendland and G. Kuhn (eds.) **1**, Springer-Verlag, (1987).

[7] M. Costabel; Boundary integral operators on Lipschitz domains: elementary results, SIAM J. Math. Anal. **19** (3), 613–626, (1998).

[8] P. Costantini, T. Lyche, C. Manni; On a class of weak Tchebycheff systems, *Numer. Math.* **101** (2005), 333–354.

[9] C. de Boor; A Practical Guide to Splines, Revised edition, Applied Mathematical Sciences 27, Springer-Verlag, New York, (2001).

[10] G. Farin; Curves and surfaces for CAGD. A practical guide, Fifth edition, Morgan Kaufmann, (2002).

[11] G. Farin, J. Hoschek and M.-S. Kim; Handbook of computer aided geometric design, Elsevier, Amsterdam, (2002.)

[12] R. T. Farouki and T. Sakkalis; Real rational curves are not "unit speed", CAGD **8** (1991), 151–157.

[13] T.J.R. Hughes, The Finite Element Method, Dover Publications, (2000).

[14] T.J.R. Hughes, J.A. Cottrell , Y. Bazilevs; Isogeometric analysis: CAD, finite elements, NURBS, exact geometry and mesh refinement, *Comput. Methods Appl. Mech. Engrg.*, **194**, 4135–4195, (2005).

[15] B.I. Kvasov, P. Sattayatham; GB-splines of arbitrary order, *J. Comput. Appl. Math.* **104** (1999), 63–88.

[16] K. Li, X. Qian; Isogeometric analysis and shape optimization via boundary integral, *Comput. Aided Design*, **43**, 1427-1437, (2011).

[17] C. Manni, F. Pelosi, M. L. Sampoli; Generalized B-splines as a tool in Isogeometric Analysis, *Comput. Methods Appl. Mech. Engrg.*, **200**, 867–881, (2011).

[18] C. Manni, et al.; Isogeometric collocation methods with generalized B-splines, *Comput. Math. Appl.*, **70**, 1659–1675, (2015).

[19] M.L. Mazure; Chebyshev–Bernstein bases, *Comput. Aided Geom. Design* **16** (1999), 649–669.

[20] S. Natarajan, J. Wang, C. Song, C. Birk, Isogeometric analysis enhanced by the scaled boundary finite element method, *Comput. Methods Appl. Mech. Engrg*, **283**, 733-762, (2015).

[21] B. H. Nguyen, H. D. Tran, C. Anitescu, X. Zhuang, T. Rabczuk, An isogeometric symmetric Galerkin boundary element method for two–dimensional crack problems, *Comput. Methods Appl. Mech. Engrg*, **306**, 252-275, (2016).

[22] C.G. Politis, A.I. Ginnis, P.D. Kaklis, K. Belibassakis and C. Feurer; An isogeometric BEM for exterior potential-flow problems in the plane, Proceeding of SIAM/ACM Joint Conference on Geometric and Physical Modeling, 349-354–2444, (2009).

[23] C.G. Politis, A. Papagiannopoulos, K.A. Belibassakis, P.D. Kaklis, K.V. Kostas, A.I. Ginnis and T.P. Gerostathis; An Isogeometric BEM for Exterior Potential-Flow Problems around Lifting Bodies, Proceeding of ECCM V, E. Oñate, J. Oliver and A. Huerta (Eds.), 2433–2444, (2014).

[24] Randall J. Le Veque, Finite Difference Methods for Ordinary and Partial Differential Equations, SIAM, (2007).

[25] R. Rannacher, W.L. Wendland; On the order of pointwise convergence of some boundary element methods. Part I. Operators of negative and zero order, Math. Model. Numer. Anal. **19**(1), 65-88, (1985).

[26] R. Rannacher, W.L. Wendland; Pointwise convergence of some boundary element methods. Part II. , Math. Model. Numer. Anal. **22**(2), 343–362, (1988).

[27] C. Schwab, W.L. Wendland, Kernel properties and representations of boundary integral operators, Math. Nachr. **156**, 156–218, (1992).

[28] R.N. Simpson, S.P.A. Bordas, J. Trevelyan, T. Rabczuk; A two-dimensional Isogeometric Boundary Element Method for elastostatic analysis,

Comput. Methods Appl. Mech. Engrg., **209-212**, 87–100, (2012).
[29] S. Sirtori, G. Maier, G. Novati, S. Micoli, A Galerkin symmetric boundary element method in elasticity: formulation and implementation, Internat. J. Numer. Methods Eng. **35**, 255–282, (1992).
[30] G. Wang, M. Fang; Unified and extended form of three types of splines, *J. Comp. Appl. Math.* **216** (2008), 498–508.
[31] W.L. Wendland; On some mathematical aspects of boundary element methods for elliptic problems, in: The Mathematics of Finite Elements and Applications V, Academic Press, London, (1985).
[32] W.L. Wendland, Variational Methods for BEM, in: L.Morino, R.Piva (eds) *Boundary Integral Equation Methods -Theory and Applications*, Springer-Verlag, (1990).